

# Software calibration for AK8963 magnetometer based on optimal ellipsoidal fitting

Aziz El fatimi, Adnane Addaim, Zouhair Guennoun

Smart Communications Research Team, University Center for Research in Space Technologies, Mohammadia School of Engineering, Mohammed V University, Rabat, Morocco

## Article Info

### Article history:

Received Apr 29, 2022

Revised Sep 10, 2022

Accepted Oct 1, 2022

### Keywords:

AK8963 Magnetometer

Earth's magnetic field

Ellipsoidal fitting

MPU-9250

Software calibration

STM32-Nucleo

## ABSTRACT

With the rapid development of mechatronics, systems in package (SiP), in particular the MPU-9250 inertial measurement Unit 9DOF (MPU-6050 6DOF and AK8963 3DOF), are becoming ubiquitous in applications for autonomous navigation purposes. Nevertheless, they suffer from some accuracy problems related to axis misalignment, disturbances, and deviation over time that make them unable to work autonomously for a long time. This paper will present a simple and practical calibration method using a least-squares based ellipsoid fitting method to calibrate and compensate for the error interference of the AK8963 sensor. Towards the end of this paper, a comparison between before and after the calibration is presented to study the software compensation effect and the stability of the magnetic sensor under study.

This is an open access article under the [CC BY-SA](#) license.



## Corresponding Author:

Aziz El fatimi

Smart Communications Research Team, University Center for Research in Space Technologies, Mohammadia School of Engineering, Mohammed V University

Rabat, Morocco

Email: azizelfatimi@research.emi.ac.ma

## 1. INTRODUCTION

As for the gravitational field, the magnetic field, also called the geomagnetic field, is an intrinsic property inherent to the Earth. The Earth's magnetic field is a vector field that is defined at any point in space by its magnitude (expressed, generally, in Gauss (G) or Tesla (T)), a direction, and a sense [1], [2]. According to the National Oceanic and Atmospheric Administration, the Earth behaves like a giant bar magnet. The direction of the geomagnetic field is similar to a magnetic field produced by a bar magnet, but with inverted poles according to Figure 1, i.e. on the axis of rotation of the Earth. Indeed, the magnetic south pole is close to the geographic north pole and the magnetic north pole is close to the geographic south pole. According to Figure 1, about 90% of the magnetic field is generated from the Earth's outer core, with a relatively small variation in intensity and position over time [3]. Its origins of appearance have been revealed for hundreds of millions of years [2], [4].

The True North Pole represents true North, and the Earth's magnetic field lines start at the True South Pole and end at the True North Pole [5], [6]. Its direction is from the magnetic south pole to the magnetic north pole. It should be noted that the magnetic north direction does not coincide with the true north direction, and there is an included angle called the declination angle. The geomagnetic intensity at any point on the Earth's surface can be represented by the geomagnetic vector  $\vec{F}$ , and its magnitude and direction are represented by the seven elements of geomagnetism ( $\vec{F}$ ,  $F_h$ ,  $D$ ,  $I$ ,  $F_x$ ,  $F_y$ ,  $F_z$ ), as shown in Figure 2 [7].

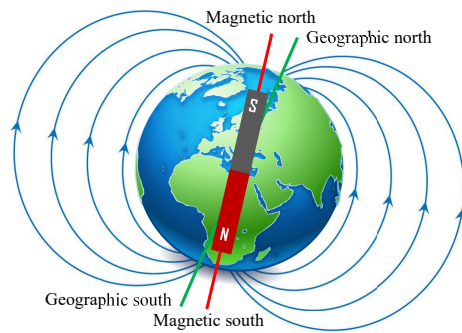


Figure 1. An illustration of the Earth's magnetic field lines and a simple bar magnet

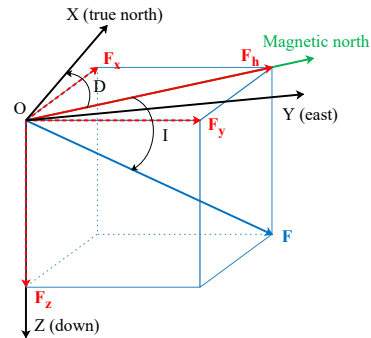


Figure 2. Schematic diagram of geomagnetic elements

In Figure 2, point O is a stationary point on the Earth. The X-axis is parallel to the line of geographic longitude and directed north; the Y-axis is parallel to the line of geographic latitude and oriented towards the east; the Z-axis is perpendicular to the ground plane; its positive direction is directed downward.  $\vec{F}$  is the geomagnetic vector, and the projection  $F_h$  of  $\vec{F}$  on the  $XOY$  plane is called the geomagnetic horizontal component;  $F_x$ ,  $F_y$ ,  $F_z$  are the components of the geomagnetic vector in the north, east, and vertical directions; the angle  $D$  between  $F_h$  and the direction of true north is called the magnetic declination; the angle  $I$  between the plane  $XOY$  and  $F$  is called the magnetic tilt angle. Furthermore, several mathematical models exist, such as the international geomagnetic reference model (IGRF) [8] and the worldwide geomagnetic model (WMM) [9], that can deduce the seven geomagnetic elements from the longitude, latitude, and altitude of a given location. Table 1 presents the seven elements of the magnetic field of the city of Rabat (latitude = 33.9692851 N, longitude = 6.8922822 W, height = 75 m), taken by the two models (WMM) [10] and (IGRF) [11].

On the other hand, several types of non-contact sensors, called magnetometers, can determine the components of the Earth's magnetic field. The magnetometer is an instrumentation device that is mainly composed of a physical element sensitive to the magnetic field which transforms the variation of a magnetic quantity into a variation of an electrical quantity, of a conditioner which maintains the optimal functioning of the sensor, and of a signal processing unit which recovers the useful signal of the electrical quantity [12], [13]. In general, magnetic sensors are used in many fields for navigation purposes; such as unmanned aerial vehicles (UAV), autonomous vehicles (AVS), drones, robots, and spacecraft. Magnetometers are often used to establish the directional heading of a craft to allow navigation between two geographical points. An accurate heading is important for successful navigation. Since magnetometers are imperfect and the Earth's magnetic field varies in different locations, calibration is required to ensure heading accuracy.

The remaining parts of this paper are organized into three sections. The first section deals with the basic notions of the magnetometer and the elliptical method adopted for its calibration. The second section describes the hardware means used during the experiment to determine the soft and hard error compensation parameters. The last section presents the analysis of the experimental results obtained in the static and dynamic states.

Table 1. Magnetic field of Rabat city [10, 11]

Model	D [nT]	I [nT]	$F_x$ [nT]	$F_y$ [nT]	$F_h$ [nT]	$F_z$ [nT]	F [nT]
IGRF	-1.007	46.065	28027	-493	28031	29094	40401
WMM	-1.003	46.061	28030	-491	28035	29093	40402

## 2. RESEARCH METHOD

Some known calibration methods using Helmholtz coils require placing the magnetometers to be calibrated in an area where a homogeneous magnetic field is created by the Helmholtz coils. These techniques have the disadvantage that it becomes necessary to use coils with a very large radius to be able to calibrate the magnetometer, which poses space problems [14]–[18]. In addition, other methods have the advantage of calibrating the magnetometer in its environment of use. For example, the Merayo technique, which is both precise and simple to implement, does not require a specific place or tools [19, 20].

## 2.1. Magnetometer model

The Earth's magnetic field is always given in the Cartesian coordinate system  $(\vec{i}, \vec{j}, \vec{k})$  by (1), as shown in Figure 2, with  $F_x$ ,  $F_y$ , and  $F_z$  representing the North, East, and Vertical components of the magnetic field vector.

$$\vec{F} = F_x \vec{i} + F_y \vec{j} + F_z \vec{k} \quad (1)$$

In the literature, several works have been carried out on the modeling of the measurements coming from the magnetometer. Current models make it possible to determine and identify the various errors in the measurements of a magnetic sensor. Generally, the main sources of errors can be separated into two forms external and internal to the sensor. Those due to disturbances in the magnetic fields around the sensor (magnetic distortion), and those caused by manufacturing defects (instrumentation errors) [19], [21]–[23]. Consequently, the approximate model for a magnetometer can be modeled as (2) (the influence of temperature on the measurements from the magnetometer is not taken into account in this model):

$$\tilde{\vec{F}} = \epsilon_{no} \cdot \epsilon_{sf} \cdot \epsilon_{ms} \left( \epsilon_{si} \cdot \vec{F} + \epsilon_{hi} \right) + \omega_b + \omega_\eta \quad (2)$$

where  $\tilde{\vec{F}}$  is the Earth's magnetic field vector measured by the magnetometer,  $\epsilon_{no}$  is the non-orthogonality error matrix,  $\epsilon_{sf}$  is the scale factor error matrix,  $\epsilon_{ms}$  is the misalignment error matrix,  $\epsilon_{si}$  is the soft iron error matrix,  $\vec{F}$  is the real vector of the Earth's magnetic field,  $\epsilon_{hi}$  is the hard iron error vector,  $\omega_b$  is the measurement bias vector, and  $\omega_\eta$  is the vector of stochastic type errors representing white noise.

## 2.2. Algorithm formulation

Merayo *et al.* [19] propose a non-iterative magnetometer calibration algorithm that estimates bias, scaling, and misalignment errors based on magnetometer measurements taken in multiple random orientations. Plotting the measurements of the three axes in a Cartesian system results in an ellipsoid, while perfect measurements result in a sphere centered around the origin (0,0,0) [19]. Calibration, therefore, consists of determining the parameters of the ellipsoid given by (3):

$$(v - c)^T A (v - c) = k \quad (3)$$

where  $v = (x, y, z)$  is a triaxial magnetometer measurement,  $c = (x_0, y_0, z_0)$  is the center of the ellipsoid,  $A = (A_{i,j})_{1 \leq i \leq 3, 1 \leq j \leq 3}$  is a positive definite matrix with real coefficients. Its eigenvectors define the axes of the ellipsoid, and its eigenvalues are equal to the inverse of the square of the semi-axes [24], and  $k > 0$ .

To find the previous parameters, the equation of the ellipsoid will be rewritten in quadratic form. The (3) becomes (4):

$$\begin{bmatrix} x - x_0 & y - y_0 & z - z_0 \end{bmatrix} \begin{bmatrix} A_{11} & A_{12} & A_{13} \\ A_{21} & A_{22} & A_{23} \\ A_{31} & A_{32} & A_{33} \end{bmatrix} \begin{bmatrix} x - x_0 \\ y - y_0 \\ z - z_0 \end{bmatrix} = k \quad (4)$$

The development of the (4) gives the expression (5):

$$\begin{aligned} & (x - x_0)^2 A_{11} + (y - y_0)^2 A_{22} + (z - z_0)^2 A_{33} + (x - x_0)(y - y_0)(A_{21} + A_{12}) + \\ & (x - x_0)(z - z_0)(A_{31} + A_{13}) + (y - y_0)(z - z_0)(A_{32} + A_{23}) = k \end{aligned} \quad (5)$$

Including the constants  $(C_{ij})_{1 \leq i \leq 3, 1 \leq j \leq 3} \in \mathbb{R}$  in (5) gives a more simplified form.

$$C_{11}x^2 + C_{22}y^2 + C_{33}z^2 + C_{12}xy + C_{13}xz + C_{23}yz + C_1x + C_2y + C_3z + C_0 = k \quad (6)$$

In matrix notation, (6) becomes:

$$\begin{bmatrix} x^2 & y^2 & z^2 & xy & xz & yz & x & y & z \end{bmatrix} \begin{bmatrix} C_{11} & C_{22} & C_{33} & C_{12} & C_{13} & C_{23} & C_1 & C_2 & C_3 \end{bmatrix}^T = k - C_0 \quad (7)$$

We apply the formula (8) which simplifies the expression (7).

$$\begin{bmatrix} x^2 & y^2 & z^2 & xy & xz & yz & x & y & z \end{bmatrix} p = 1 \quad (8)$$

where  $p$  is a vector of parameters ( $9 \times 1$ ) to be estimated. Merayo *et al.* [19] prove that  $U$  is an upper triangular ( $3 \times 3$ ) matrix can be found by a Cholesky factorization of a positive definite matrix formed by the elements of  $p$ :

$$A = U^T U = \begin{bmatrix} p_1 & p_4/2 & p_5/2 \\ p_4/2 & p_2 & p_6/2 \\ p_5/2 & p_6/2 & p_3 \end{bmatrix} \quad (9)$$

The estimation of the parameters of the vector  $p$  requires at least nine measurements in different orientations. The (8) can then be rewritten as (10):

$$Dp = 1 \quad (10)$$

where  $D$  is a matrix containing the  $N$  magnetometer measurements along the  $x$ ,  $y$ , and  $z$  axes. We will then have:

$$D = \begin{bmatrix} x_1^2 & y_1^2 & z_1^2 & x_1 y_1 & x_1 z_1 & y_1 z_1 & x_1 & y_1 & z_1 \\ x_2^2 & y_2^2 & z_2^2 & x_2 y_2 & x_2 z_2 & y_2 z_2 & x_2 & y_2 & z_2 \\ \vdots & \vdots \\ x_N^2 & y_N^2 & z_N^2 & x_N y_N & x_N z_N & y_N z_N & x_N & y_N & z_N \end{bmatrix} \quad (11)$$

The solution for the least squares estimation problem is given by (12).

$$p = [D^T D]^{-1} D^T \quad (12)$$

To make accurate estimates, a large number of measurements should be considered, which requires computational power and precision to calculate  $[D^T D]^{-1}$ . This problem can be avoided by reformulating (10) as (13):

$$D^* p^* = 0 \quad (13)$$

where  $D^*$  contains  $N$  magnetometric measurements, reinforced by a column of units:

$$D^* = \begin{bmatrix} x_1^2 & y_1^2 & z_1^2 & x_1 y_1 & x_1 z_1 & y_1 z_1 & x_1 & y_1 & z_1 & 1 \\ x_2^2 & y_2^2 & z_2^2 & x_2 y_2 & x_2 z_2 & y_2 z_2 & x_2 & y_2 & z_2 & 1 \\ \vdots & \vdots \\ x_N^2 & y_N^2 & z_N^2 & x_N y_N & x_N z_N & y_N z_N & x_N & y_N & z_N & 1 \end{bmatrix} \quad (14)$$

and  $p^*$  is now a vector of ( $10 \times 1$ ). The solution of the homogeneous equation can be computed efficiently by a singular value decomposition (SVD), which is detailed in [25]. The center of the ellipsoid is calculated by (15).

$$c = A^{-1} \begin{bmatrix} p_7 \\ p_8 \\ p_9 \end{bmatrix} \quad (15)$$

After determining  $c$  and  $U$ , a calibrated measurement  $w$  can be calculated by (16).

$$w = U(v - c) \quad (16)$$

## 2.3. Hardware configuration

### 2.3.1. MPU-9250

Invensense Technology's MPU-9250 is a system in package (SiP) combining two chips. It is composed of an MPU-6050 and an AK8963 magnetometer. It, therefore, has the six axes of the MPU-6050 (3 for the accelerometer and 3 for the gyroscope) and the three axes of the magnetometer. This kind of circuit is also called an inertial measurement unit (IMU-9DOF) [26]. The MPU-9250 is connected to the STM32 Nucleo 64 acquisition board via a bidirectional half-duplex synchronous serial bus I2C (SDA: serial data line and SCL:

serial clock line). The Figures 3 and 4 show the rotation polarity and the orientation of the sensitivity axes for the two sensors used.

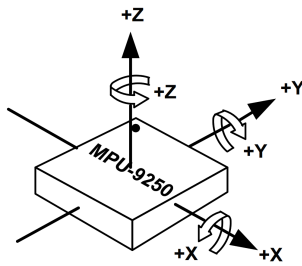


Figure 3. Orientation of the axes and rotation polarity of the gyroscope

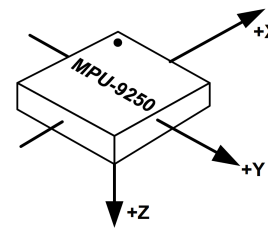


Figure 4. Orientation of the magnetometer axes

**2.3.2. STM32 Nucleo-F411RE**

The STM32 Nucleo-F411RE development board is a type of 32-bit microcontroller made by the Franco-Italian company STMicroelectronics. STM32 chips are grouped into different series of the same design, based on 32-bit ARM architecture processors, such as the Cortex-M4. It is designed to perform real-time low-voltage digital signal processing. This board is ideal for quickly creating prototypes, and its standardized connectivity makes it possible to build and reuse electronic modules on all the inputs and outputs of the Nucleo board. The PCB contains an in-circuit ST-LINK/V2-1 programmer and a debugger, which can be used as an onboard microprocessor or in standalone mode with any other application that includes an STM32 microprocessor [27]. The STM32 Nucleo-F411RE module operates at a frequency of 100 MHz while ensuring relatively low power consumption in work, sleep, and shutdown modes. Its main characteristics are mentioned in Table 2.

Table 2. Main features of the STM32 Nucleo-F411RE board

Feature	Flash memory	SRAM memory	Operating voltage	Temperature range
Value	512 Kbytes	128 Kbytes	1.7 to 3.6 V	-40 to +125 °C

**2.3.3. Electrical scheme**

The final electrical scheme adopted for magnetometer data acquisition is shown in Figure 5. The MPU-9250 is interfaced to the STM32 through an I2C serial connection. The USB port is used to transmit and receive data between the STM32 microcontroller and the computer.

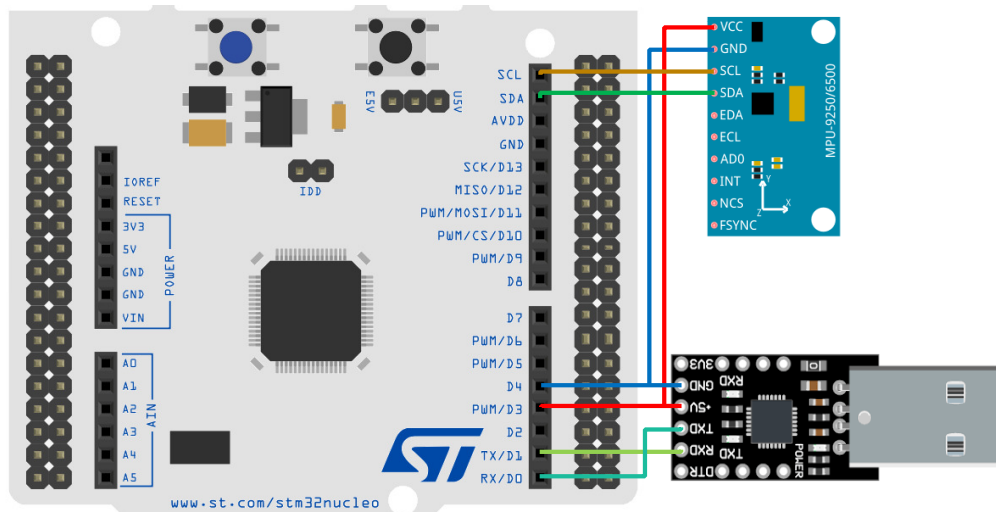


Figure 5. Electrical scheme for magnetometer data acquisition

### 3. RESULTS AND DISCUSSION

This section highlights the implementation of the ellipsoid fitting method based on the least squares method detailed in the 2.2 section to calibrate and compensate for the error interference of the AK8963 sensor. Then a comparison between before and after calibration is presented to study the effect of software compensation and the stability of the magnetic sensor under study. At the end of this section, a plan is made to check that the algorithm works correctly in both static and dynamic situations.

#### 3.1. Magnetometer calibration parameters

The calibration of magnetometers is generally carried out by collecting the magnetic field intensities in all directions in space. The final measurement data creates an ellipse in space. The problem, therefore, of calibration resides in the way of finding the center and the parameters of the ellipsoid. The Figure 6 represents 7,000 samples measurements in all directions from the AK8963 sensor. Then, the calculation of the correction factors mentioned in the section 2.2 makes it possible to recalibrate the magnetometer as accurately as possible. As shown in Figure 7, the adjustment algorithm can essentially accurately calculate the position of the center of the ellipsoid, which represents the offsets of the three axes of the magnetometer. The fitting parameters of the ellipsoid  $U$  and  $c$  are given in (17) and (18).

$$U = \begin{bmatrix} 0.0285 & 0.0004 & -0.0020 \\ 0 & 0.0325 & -0.0031 \\ 0 & 0 & 0.0304 \end{bmatrix} \quad (17)$$

and

$$c = [-1.4028 \quad 27.9710 \quad -28.1013]^T \quad (18)$$

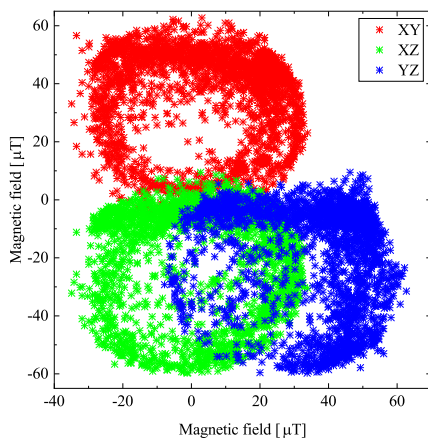


Figure 6. Original magnetometer data

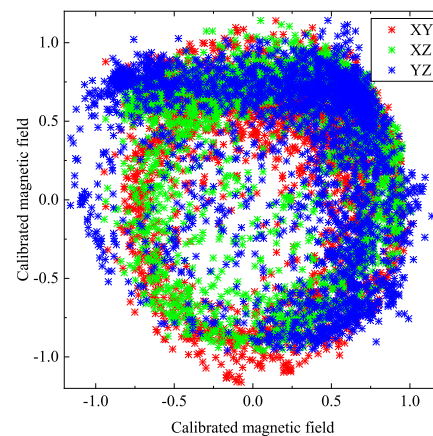


Figure 7. Compensated magnetometer data

#### 3.2. Results analysis

To better visualize the results, a uniaxial representation is used to represent the experimental data in both static and dynamic states. Figure 8 illustrates the variation of the magnetic field acquired before and after calibration along the three axes for ten seconds in a static state. The second experiment concerns the acquisition of magnetometric measurements in 3D for ten seconds in a dynamic state. The Figure 9 represents the variation evolution of the received magnetic field before and after calibration.

By comparing the data before and after calibration, it is clear to note that the two curves (calibrated and uncalibrated data) overlap throughout the measurement acquisition interval with a slight shift. In addition, it is obvious to underline that the measurements of the AK8963 magnetometer are faithful to the manufacturer's prescriptions; however, they are not correct and present a significant shift in offset specific to each axis. Using the adopted Merayo ellipsoidal algorithm, the magnetometric measurements are adjusted around the origin (0,0,0). As a result, the deformed measurements are rectified, which means that the disturbances that are due to the effects of the errors of non-orthogonality, the scale factor, of hard iron, soft iron, misalignment, and the external stochastic errors are compensated.

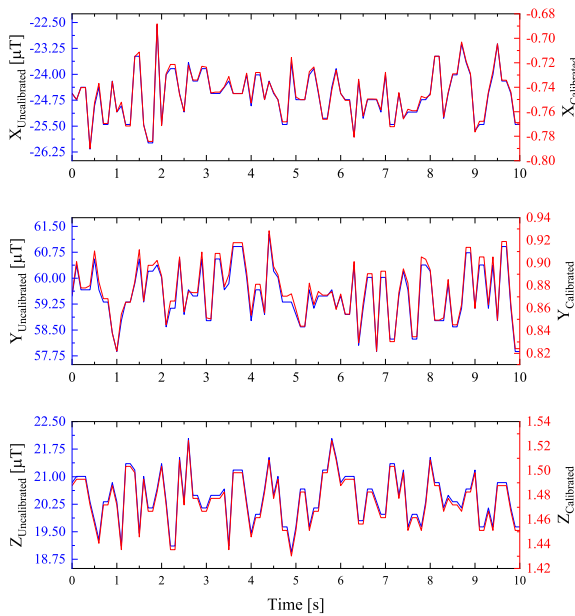


Figure 8. Magnetometer data in a static state

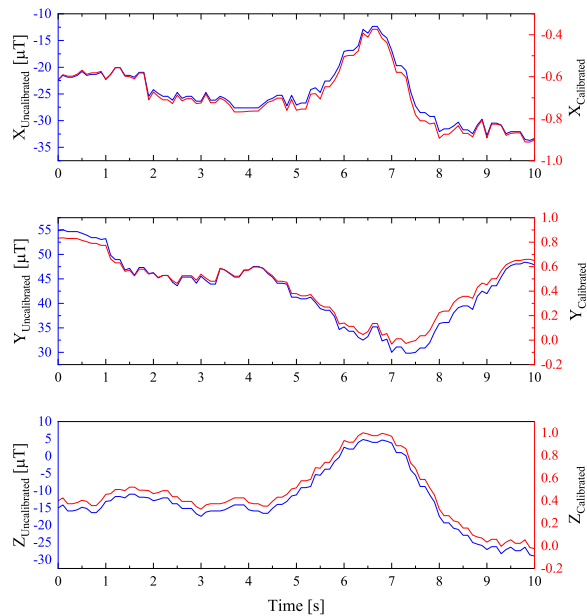


Figure 9. Magnetometer data in a dynamic state

#### 4. CONCLUSION

In summary, the objective of this work is to apply a simple and practical Merayo algorithm to fit the magnetometer measurements of a low-cost sensor (AK8963). The ellipsoidal fitting method used, based on the least-squares method, was implemented and tested to verify the validity of the procedure. After a series of experiments that were carried out under real geographical conditions, both static and dynamic, an offset shift was found and the measurements were corrupted by noise from different machining, installation, and environmental factors. The comparison before and after the calibration showed that the magnetic sensor is precalibrated at the factory and is stable during static and dynamic measurements. On the other hand, the software compensation presented above is not sufficient and requires filtering adapted to the frequency of acquisition of the measurements and the external and internal disturbances of the sensor.

#### ACKNOWLEDGEMENT

This work was carried out in the frame of the cooperation between the Royal Center for Space Research and Studies (CRERS) and the Mohammed V University in Rabat (UM5R).

#### REFERENCES

- [1] R. Lanza and A. Meloni, "The earth's magnetic field," in *The Earth's Magnetism*, Springer Berlin Heidelberg, 2006, pp. 1–66.
- [2] M. Brown, M. Korte, R. Holme, I. Wardinski, and S. Gunnarson, "Earth's magnetic field is probably not reversing," in *Proceedings of the National Academy of Sciences*, May 2018, vol. 115, no. 20, pp. 5111–5116, doi: 10.1073/pnas.1722110115.
- [3] E. Camporeale, M. D. Cash, H. J. Singer, C. C. Balch, Z. Huang, and G. Toth, "A gray-box model for a probabilistic estimate of regional ground magnetic perturbations: enhancing the NOAA operational geospace model with machine learning," *Journal of Geophysical Research: Space Physics*, vol. 125, no. 11, Nov. 2020, doi: 10.1029/2019JA027684.
- [4] A. Goguitchaichvili, R. G. Ruiz, F. J. Pavón-Carrasco, J. J. M. Contreras, A. M. S. Arechalde, and J. Urrutia-Fucugauchi, "Last three millennia earth's magnetic field strength in Mesoamerica and southern United States: Implications in geomagnetism and archaeology," *Physics of the Earth and Planetary Interiors*, vol. 279, pp. 79–91, Jun. 2018, doi: 10.1016/j.pepi.2018.04.003.

- [5] G. Oelsner *et al.*, “Integrated optically pumped magnetometer for measurements within earth’s magnetic field,” *Physical Review Applied*, vol. 17, no. 2, Feb. 2022, doi: 10.1103/PhysRevApplied.17.024034.
- [6] J. Qian, X. Chen, M. Wang, J. Ge, C. Zhou, and J. Zhang, “Measurement and modeling of magnetic declination error associated with horizontal drift,” in *International Conference on High Performance Computing and Communication (HPCCE)*, Feb. 2022, vol. 12162, doi: 10.1117/12.2628184.
- [7] T. W. Horton, R. O. Bierregaard, P. Zawar-Reza, R. N. Holdaway, and P. Sagar, “Juvenile osprey navigation during trans-oceanic migration,” *PLoS ONE*, vol. 9, no. 12, Dec. 2014, doi: 10.1371/journal.pone.0114557.
- [8] J. Baerenzung, M. Holschneider, J. Wicht, V. Lesur, and S. Sanchez, “The Kalmag model as a candidate for IGRF-13,” *Earth, Planets and Space*, vol. 72, no. 1, Dec. 2020, doi: 10.1186/s40623-020-01295-y.
- [9] W. Yu, M. Liu, L. Song, H. Li, and D. Zhu, “Analysis of main magnetic field in Chinese mainland based on WMM2020 and IGRF13,” in *International Conference on Computational Modeling, Simulation, and Data Analysis (CMSDA)*, Mar. 2022, vol. 12160, doi: 10.1117/12.2627893.
- [10] BGS, “World Magnetic Model 2020 Calculator,” *Geomagnetism British Geological Survey*, 2022. [https://www.geomag.bgs.ac.uk/data/service/models/compass/wmm\\_calc.html](https://www.geomag.bgs.ac.uk/data/service/models/compass/wmm_calc.html) (accessed Apr. 21, 2022).
- [11] “International Geomagnetic Reference Field (IGRF),” *13th Generation Calculator*, 2022. [https://www.geomag.bgs.ac.uk/data\\_service/models/compass/igrf\\_calc.html](https://www.geomag.bgs.ac.uk/data_service/models/compass/igrf_calc.html) (accessed Apr. 21, 2022).
- [12] V. V. Davydov, V. I. Dudkin, N. S. Myazin, and R. V. Davydov, “New design of a magnetometer based on nuclear magnetic resonance to study variations of the mid-field magnetic strength,” *Applied Magnetic Resonance*, vol. 52, no. 9, pp. 1201–1213, Sep. 2021, doi: 10.1007/s00723-021-01373-8.
- [13] C. F. Soon *et al.*, “Investigation of wireless magnetometer in sensing magnetic field changes at different car direction and speed,” *Bulletin of Electrical Engineering and Informatics (BEEI)*, vol. 10, no. 2, pp. 668–679, Apr. 2021, doi: 10.11591/eei.v10i2.2707.
- [14] C. Hajiyev, “In-orbit magnetometer bias and scale factor calibration,” *International Journal of Metrology and Quality Engineering*, vol. 7, no. 1, Apr. 2016, doi: 10.1051/ijmqe/2016003.
- [15] E. Sutanto, F. Chandra, E. Gonnelli, and S. Suhariningsih, “Residual current measurement using helmholtz coil configuration with different current flow,” *International Journal of Electrical and Computer Engineering (IJECE)*, vol. 8, no. 3, pp. 1432–1441, Jun. 2018, doi: 10.11591/ijece.v8i3.pp1432-1441.
- [16] B. Dahmane, B. Lejdel, E. Clementini, F. Harrats, S. Nassar, and L. H. Abderrahmane, “Controlling the degree of observability in GPS/INS integration land-vehicle navigation based on extended Kalman filter,” *Bulletin of Electrical Engineering and Informatics (BEEI)*, vol. 11, no. 2, pp. 702–712, Apr. 2022, doi: 10.11591/eei.v11i2.3695.
- [17] M. Saqib, F. S. N., and F. J. N., “Design and development of helmholtz coils for magnetic field,” in *2020 International Youth Conference on Radio Electronics, Electrical and Power Engineering (REEPE)*, Mar. 2020, pp. 1–5, doi: 10.1109/REEPE49198.2020.9059109.
- [18] A. Jaafar, N. M. Thamrin, and N. M. Zan, “Wireless sensor network calibration technique for low-altitude unmanned aerial vehicle localization in paddy field,” *Bulletin of Electrical Engineering and Informatics (BEEI)*, vol. 10, no. 1, pp. 208–215, Feb. 2021, doi: 10.11591/eei.v10i1.2512.
- [19] J. M. G. Merayo, P. Brauer, F. Primdahl, J. R. Petersen, and O. V. Nielsen, “Scalar calibration of vector magnetometers,” *Measurement Science and Technology*, vol. 11, no. 2, pp. 120–132, Feb. 2000, doi: 10.1088/0957-0233/11/2/304.
- [20] V. Petrucha, P. Kaspar, P. Ripka, and J. M. G. Merayo, “Automated system for the calibration of magnetometers,” *Journal of Applied Physics*, vol. 105, no. 7, 2009, doi: 10.1063/1.3062961.
- [21] Y. Liu, X. Li, X. Zhang, and Y. Feng, “Novel calibration algorithm for a three-axis strapdown magnetometer,” *Sensors*, vol. 14, no. 5, pp. 8485–8504, May 2014, doi: 10.3390/s140508485.
- [22] O. L. Q. Al-Mahdi, A. Y. Ahmed, J. O. Dennis, and M. H. Md. Khir, “Modeling of a highly sensitive lorentz force-based CMOS-MEMS magnetometer for e-compass applications,” in *2020 8<sup>th</sup> International Conference on Intelligent and Advanced Systems (ICIAS)*, Jul. 2021, pp. 1–4, doi: 10.1109/ICIAS49414.2021.9642619.
- [23] Z. Dang, J. Xiang, and K. Liu, “Magnetometer model used for micro satellite ground simulation of control system,” *Aerospace Shanghai*, 2011.
- [24] N. J. Higham, *Functions of matrices: theory and computation*. SIAM, 2008.
- [25] T. Svoboda, “Least-squares Solution of Homogeneous Equations supportive text for teaching purposes,” *supportive text for teaching purposes, Faculty of Electrical Engineering, Czech Technical University*. 2005.
- [26] I. Nevlydov, O. Filipenko, M. Volkova, and G. Ponomaryova, “MEMS-based inertial sensor signals and machine learning methods for classifying robot motion,” in *2018 IEEE Second International Conference on Data Stream Mining and Processing (DSMP)*, Aug. 2018, pp. 13–16, doi: 10.1109/DSMP.2018.8478613.
- [27] P. Visconti, B. Sbarro, P. Primiceri, R. De Fazio, and A. Lay-Ekuakille, “Design and testing of an electronic control system based on stm x-nucleo board for detection and wireless transmission of sensors data applied to a single-seat formula sae car,” *International Journal of Electronics and Telecommunications*, vol. 65, no. 4, pp. 671–678, 2019, doi: 10.24425/ijet.2019.130248.

**BIOGRAPHIES OF AUTHORS**

**Aziz El fatimi**     was born in Kelaa of Sraghnas, Morocco in 1985. He received the Engineer degree in Electromechanical Engineering in 2015 and the Ph.D. degree in Electrical and Telecommunications Engineering in 2021 from the Ecole Nationale Supérieure d'Arts & Métiers of Meknes in Morocco. He is currently a Ph.D. student in Aerospace Technologies at the University Center for Research in Space Technologies at Ecole Mohammadia d'Ingénieurs of Rabat in Morocco. His research is focused on algorithms, modeling and control of multi-physical systems, full-wave analysis, and microstrip patch antennas. He can be contacted at email: azizelfatimi@research.emi.ac.ma.



**Adnane Addaim**     received his Master degree in 2001 and his Ph.D. degree in 2008, both in Satellite Communication from Mohammadia School of Engineers (EMI) at Mohammed V University in Rabat, Morocco. From 2002 to 2003, he was employed at SIEMENS.AG as Transmission Engineer then as responsible of the implementation of the supervision network of the Meditelecom GSM Microwave Network, in Morocco. He was recipient of the first prize of the best Ph.D. thesis between 2007 and 2009 in the field of Sciences and technologies at Mohammed V University. From 2010 to 2020, he was a professor lecture at ENSA Engineering School at Kenitra, Morocco. From 2021, he is a full professor at the EMI Engineering School at Rabat, Morocco. His current research interests include signal processing, satellite communication systems wireless and Nanosatellite system engineering. He can be contacted at email: addaim@emi.ac.ma.



**Zouhair Guennoun**     received the B.Eng. degree in electrical engineering in 1987 from ULG, Liege Belgium, M.Sc. degrees in Electrical and Computer Engineering in 1993 from École Mohammadia d'Ingénieurs (EMI), Rabat, and the Ph.D. degree in Applied Science in 1996 from EMI. He is currently a Professor of Computer and electronic Engineering at École Mohammadia d'Ingénieurs (EMI) where he is member of the ERSC formerly known as LEC, and member of the spatial research center (CRES). His research interests include wireline and wireless networks, advanced communications systems, signal processing, audio and image compression, audio cryptography. He is a senior member of IEEE. He can be contacted at email: zouhair@emi.ac.ma.